Published by :
https://www.ijert.org/
An International Peer-Reviewed Journal

International Journal of Engineering Research & Technology (IJERT)
ISSN: 2278-0181
Vol. 15 Issue 04 , April - 2026

Soft Switching Dual Active Bridge Converter for Charging System

Duc-Tuan Do
Dr, Department of Electrical Engineering
Thainguyen University of Technology
Thai Nguyen, Vietnam

Van-Nghiep Dinh
Dr, Department of Electrical Engineering
Thainguyen University of Technology
Thai Nguyen, Vietnam

***Abstract*—This paper presents a dual-active-bridge (DAB) structure enabling bidirectional power transmission. With its two-stage energy conversion, this converter offers several outstanding advantages for high-power applications, particularly its zero-voltage switching capability (ZVS). The research focuses on a detailed analysis of the converter structure, including its operating principle, soft switching characteristics, steady-state mode, output characteristics, and control strategy, with a focus on applications in electric vehicle charging infrastructure. Additionally, a simulation model of the DAB structure with a maximum power of 10 kW was built on the PSIM platform, and the obtained results are presented and analyzed comprehensively.**

***Keywords*— Soft Switching; Dual-active-bridge converter; Charging system; Constant voltage; Constant current.**

I. INTRODUCTION

dual-active-bridge (DAB) converters are widely used in many applications [1]-[3], for example: battery and accumulator management systems [4], electric vehicles [5], semiconductor transformers [6]. The literature mainly analyzes the steady-state operating conditions as well as the mathematical description of the converter, but has not clearly analyzed the soft switching process (ZVS) as one of the factors contributing to improving the efficiency of the converter in the systems [7]-[10].

In [7], the low-order model of the DAB converter is presented with the advantage of very high large and small signal accuracy in common applications, simple, and easy to understand. However, this low-order model still has some disadvantages, such as the accuracy may decrease under more complex operating conditions or modulation techniques.

The equivalent circuit model of the DAB converter is presented in document [8] with advantages such as: helping the reader to better understand the physical nature of the converter; convenient for analyzing all transfer functions; can accurately reproduce both the steady state and the large signal transient state of the original system. However, the inference of the model can be very complex, which is one of the disadvantages of this method.

In document [9]-[11], the energy-shaping-based model is presented with the advantages: it can resolve the conflict between speed and overshoot, is more efficient than traditional PI controllers, and has strong noise immunity. However, this method still has some disadvantages, such as a more complex control strategy in design compared to traditional linear methods.

The DAB converter for fast-charging of battery electric vehicles is presented in [12]. However, the operating principle of the DAB converter is not discussed.

From the above analysis, to clarify the working process of the DAB converter for a charging system with different description methods, a clear analysis of the operating states is necessary, which provides the reader with a clearer understanding of the soft switching process of the switches in the converter.

II. OPERATION PRINCIPLE

A. Analysis of the operating states of the DAB converter

A dual-active-bridge converter for a charging system is shown in Fig.1. The operation principle of the DAB converter is eight states.

State 1 [t_0-t_1] at time t_0 switches S_1 and S_4 start conducting, while switches S_6 and S_7 are conducting as shown in Fig 2(a). The output voltage of the primary transformer v_{T1} is positive, and the output voltage of the secondary transformer v_{T2} is negative, as shown in Fig 3. Therefore, a positive voltage is applied to the inductor L, the current through the inductor increases linearly and is given by (1).

$$i(1) = \frac{V_1 + nV_2}{L} \frac{\phi}{2\pi} T_s + i(t_0) \quad (1)$$

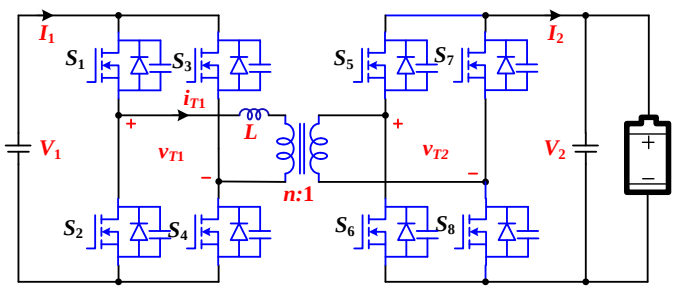

Fig. 1. Dual-active-bridge (DAB) converter for charging system.

This research was financially supported by the Program of the Ministry of Education and Training of Vietnam under grant number B2024-TNA-17.

International Journal of Engineering Research & Technology (IJERT)
ISSN: 2278-0181
Vol. 15 Issue 04 , April - 2026

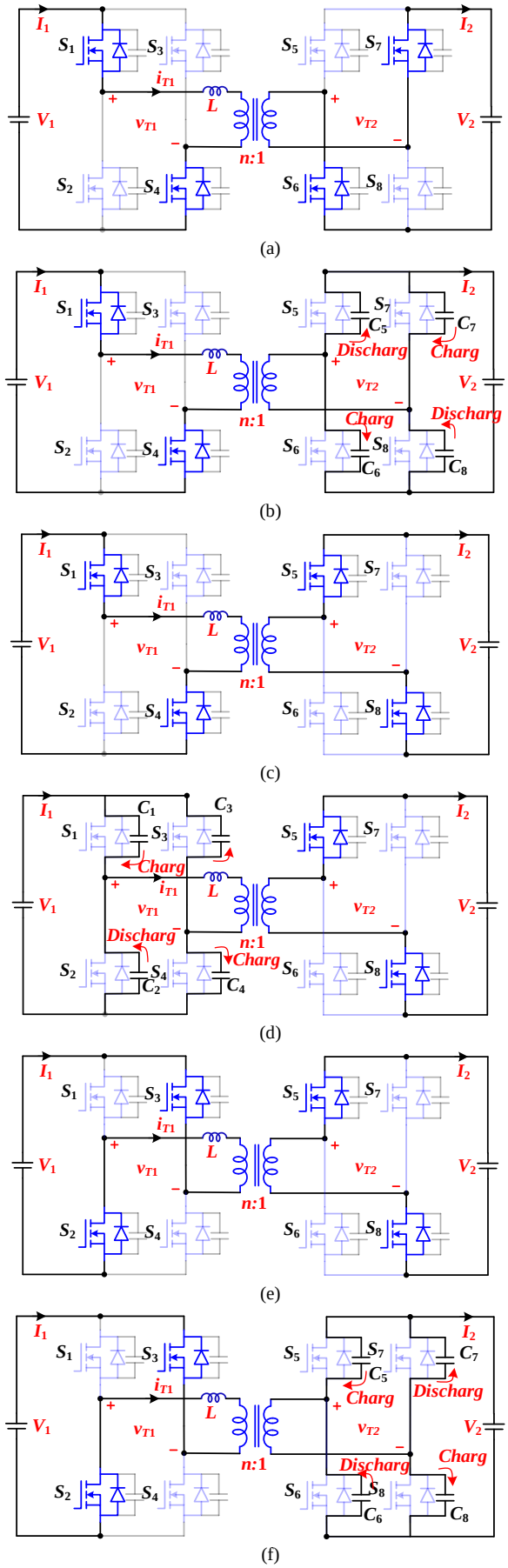

Fig. 2. Equivalent circuit of the DAB converter: a) State 1, b) State 2, c) State 3, d) State 4, e) State 5, f) State 6, g) State 7, h) State 8.

State 2 [t_1-t_2] at time t_1 switches S_6 and S_7 begin to lock, while switches S_1 and S_4 are conducting as shown in Fig. 2(b). The energy accumulated in inductance L at time t_1 charges capacitors C_6 and C_7, and capacitors C_5 and C_8 discharge. The output voltage on the secondary side of the transformer v_{T2} increases from $-nV_2$ to $+nV_2$ as shown in Fig. 3. If the energy accumulated in inductance L is sufficient to complete the charging and discharging process of the capacitors, then soft switching will be achieved when S_5 and S_8 begin to conduct at time t_2. No energy is transferred from the primary to the secondary during this time.

State 3 [t_2-t_3] at time t_2 switches S_5 and S_8 start conducting, while S_1 and S_4 are conducting as shown in Fig. 2(c). The output voltage on the primary side of the transformer v_{T1} is positive, and the output voltage on the secondary side of the transformer v_{T2} is also positive. If voltage V_1 is greater than or equal to the voltage value of V_2 applied back to the primary side of the transformer, then the current through inductor L increases linearly as shown in Fig. 3(a). Conversely, the current through inductor L decreases linearly as shown in Fig. 3(b). The current through inductor L is given by (2).

$$i(2) = \frac{V_1 - nV_2}{L}\frac{1-\phi}{2\pi}T_s + i(t_2) \qquad (2)$$

State 4 [t_3-t_4] at time t_3 switches S_1 and S_4 begin to lock at the most positive value of the current through the inductor, while switches S_5 and S_8 are conducting as shown in Fig. 2(d). The energy accumulated in inductor L at time t_3 charges capacitors C_1 and C_4, and capacitors C_2 and C_3 discharge. The primary voltage of the transformer v_{T1} decreases from $+V_1$ to $-V_1$ as shown in Fig. 3. If the energy accumulated in inductor L is sufficient to complete the charging and discharging process of the capacitors, soft switching will be achieved when S_2 and S_3 begin to conduct at time t_4. No energy is transferred from primary to secondary during this time.

International Journal of Engineering Research & Technology (IJERT)
ISSN: 2278-0181
Vol. 15 Issue 04 , April - 2026

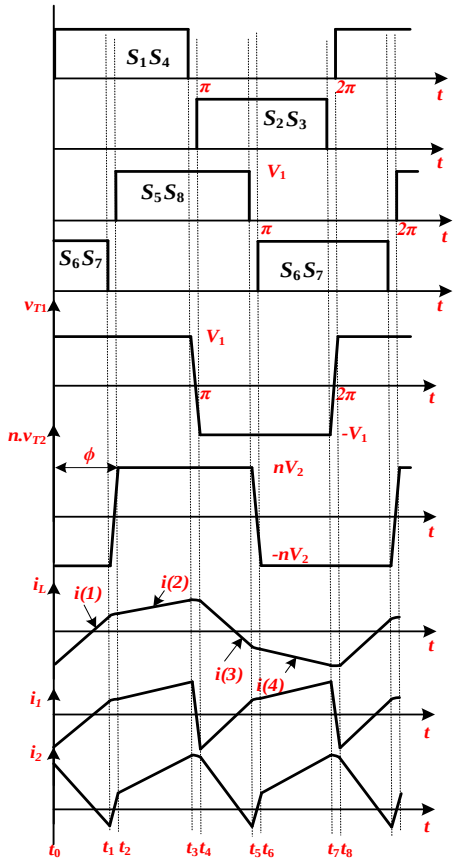

(a)

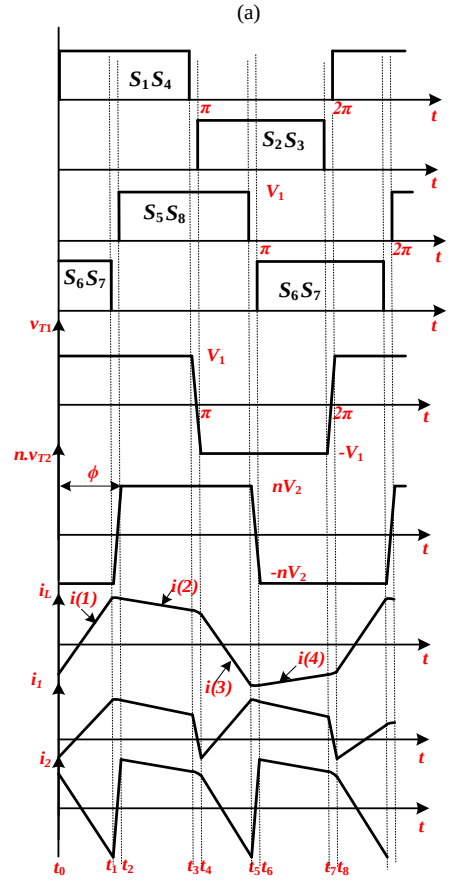

(b)

Fig. 3. Primary and secondary voltage waveforms of the transformer: a) when $V_1 \geq nV_2$ and b) when $V_1 < nV_2$

State 5 [t_4-t_5] at time t_4 while switches S_5 and S_8 are conducting, switches S_2 and S_3 start conducting, the equivalent circuit diagram is shown in Fig. 2(e). The output voltage on the primary side of the transformer v_{T1} is negative, the output voltage on the secondary side of the transformer v_{T2} is positive, as shown in Fig. 3. Therefore, the voltage applied to the inductor L is negative, the current through the inductor L decreases linearly and is given by (3).

$$i(3) = \frac{-V_1 + nV_2}{L}\frac{\phi}{2\pi}T_s + i(t_4) \qquad (3)$$

State 6 [t_5-t_6] at time t_5 switches S_5 and S_8 begin to lock, while switches S_2 and S_3 are conducting as shown in Fig. 2(f). The energy accumulated in inductance L at time t_5 charges capacitors C_5 and C_8, and capacitors C_6 và C_7 discharge. The output voltage on the secondary side of the transformer v_{T2} decreases from $+nV_2$ to $-nV_2$ as shown in Fig. 3. If the energy accumulated in inductance L is sufficient to complete the charging and discharging of the capacitors, then soft switching (ZVS) will be achieved when S_6 and S_7 begin to conduct at time t_6. No energy is transferred from the primary to the secondary during this time.

State 7 [t_6-t_7] at time t_6 switches S_6 and S_7 are given control signals to open while switches S_2 and S_3 are conducting, the equivalent circuit diagram is shown in Fig. 2(g). The output voltage on the primary side of the transformer v_{T1} is negative, the output voltage on the secondary side of the transformer v_{T2} is also negative as shown in Fig. 3. If voltage V_1 is greater than or equal to the voltage value of V_2 applied back to the primary side of the transformer, then the current through inductor L decreases linearly as shown in Fig. 3(a). Conversely, the current through inductor L increases linearly as shown in Fig. 3(b). The current through inductor L is given by (4).

$$i(4) = \frac{-V_1 - nV_2}{L}\frac{1-\phi}{2\pi}T_s + i(t_6) \qquad (4)$$

State 8 [t_7-t_8] at time t_7 switches S_2 and S_3 begin to lock at the most negative value of the current through the inductor, while switches S_6 and S_7 are conducting as shown in Fig. 2(h). The energy accumulated in the inductor L at time t_7 charges capacitors C_2 and C_3, and capacitors C_1 and C_4 discharge. The primary voltage of the transformer v_{T1} increases from $-V_1$ to $+V_1$ as shown in Fig. 3. If the energy accumulated in the inductor L is sufficient to complete the charging and discharging process of the capacitors, soft switching will be achieved when S_1 and S_2 begin to conduct at time t_8. No energy is transferred from the primary to the secondary during this time.

B. PI controller design

Although the performance of a PI controller depends on the algebraic selection system, it is still widely used in industry as a typical form of linear control. This is because PI controllers can achieve high accuracy standards, operate stably in noisy environments, and possess a simple structure that is easy to develop and implement. The PI controller is characterized by a pole at the origin along with a zero point, and can be represented as follows:

International Journal of Engineering Research & Technology (IJERT)
ISSN: 2278-0181
Vol. 15 Issue 04 , April - 2026

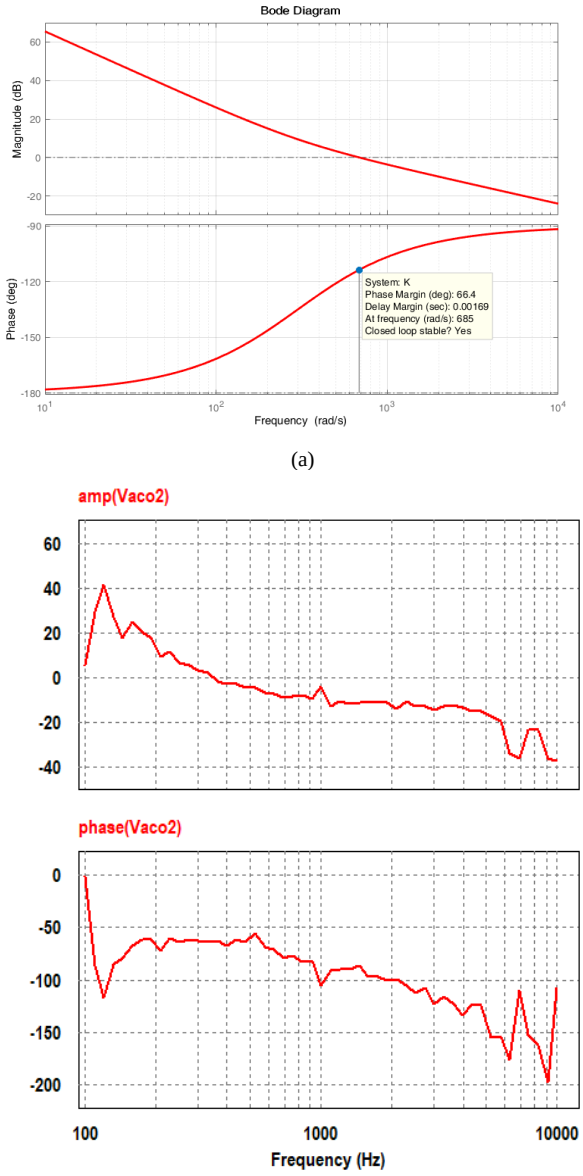

(a)

(b)

Fig. 4. Bode plot of PI controller: a) Drawing using MATLAB software, b) Drawing using PSIM software.

$$G_{PI}(S) = K_{PI}\frac{\left(1+\frac{s}{\omega_{PI,z}}\right)}{s} \quad (5)$$

In this case, $\omega_{PI,z}$ is the angular frequency of the unique zero, and k_{PI} is the DC gain.

Fig. 4 presents the Bode plot of the PI controller, constructed on the derived transfer function in (5), where the phase margin (PM) amplitude reaches 66° in the high-frequency region, the f_c = 100 Hz (628 rad/s), K_{pi} =13.65, $\omega_{pi,z}$ = 300 rad/s.

III. Simulation Results

To verify the working principle analysis, the authors used PSIM software to simulate the system. The simulation was performed in two cases: when $V_1 \geq nV_2$ and when $V_1 < nV_2$. The circuit parameters are given in Table 1.

TABLE I. Parameters of the Elements in the DAB Converter

V_1	f_1	L	V_2	I_2	P_o	R_{load}	n
750 V	100 kHz	58.6 µH	250 V	20A	5 kW	12.5 Ω	10/6
750 V	100 kHz	58.6 µH	500 V	20 A	10 kW	25 Ω	10/6

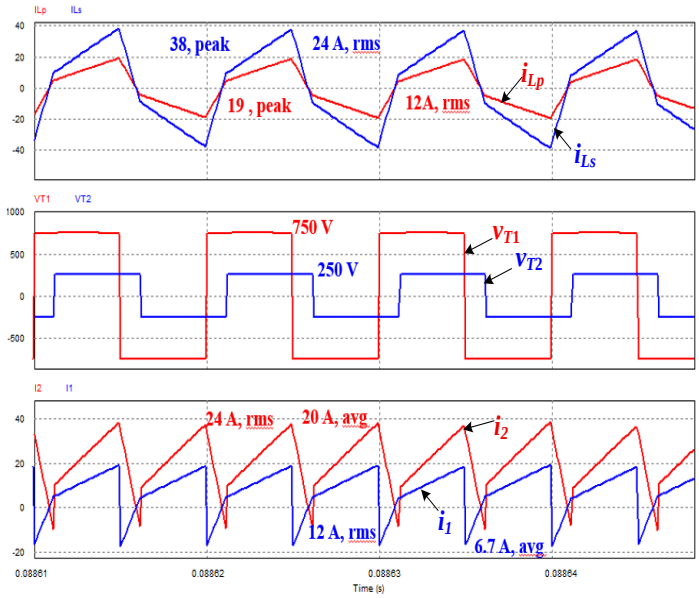

Fig. 5. Simulation results when $V_1 \geq nV_2$

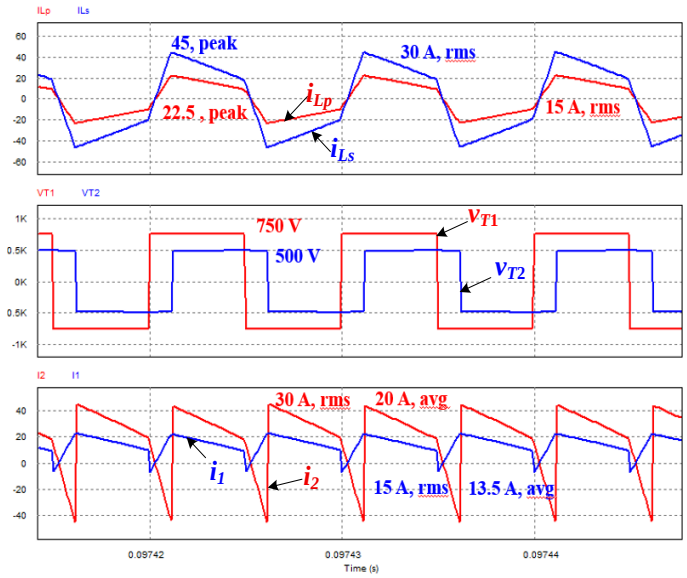

Fig. 6. Simulation results when $V_1 < nV_2$

The primary and secondary currents in the transformer are shown at the top of Figs 5 and 6. Meanwhile, the primary and secondary voltages in the transformer are shown in the middle of Figs. 5 and 6. The top of Figs 5 and 6 presents the input and output current of the DAB converter.

International Journal of Engineering Research & Technology (IJERT)
ISSN: 2278-0181
Vol. 15 Issue 04 , April - 2026

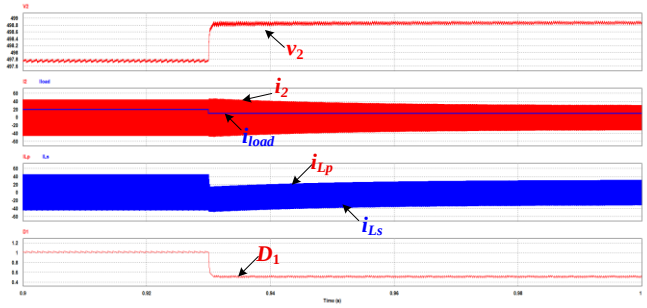

Fig. 7. Simulation results of CV mode when the load changes 25-50Ω

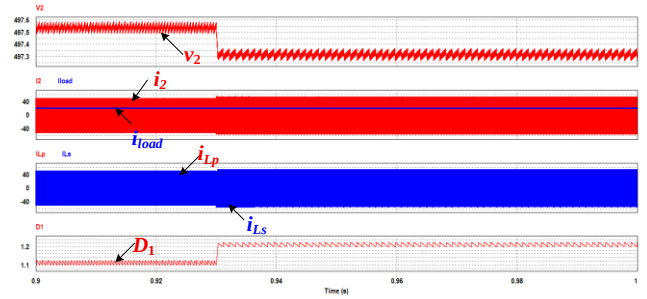

Fig. 8. Simulation results of CV mode when the input source changes 800-700V.

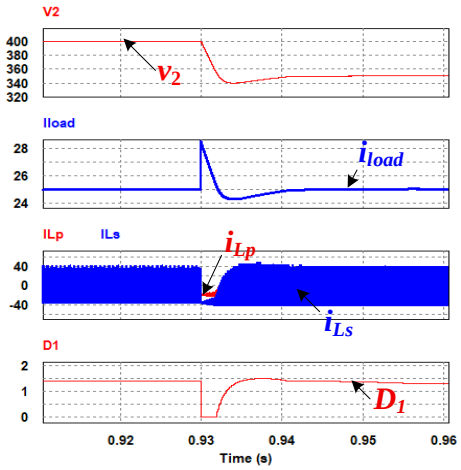

Fig. 9. Simulation results of CC mode when the load changes 16-14Ω

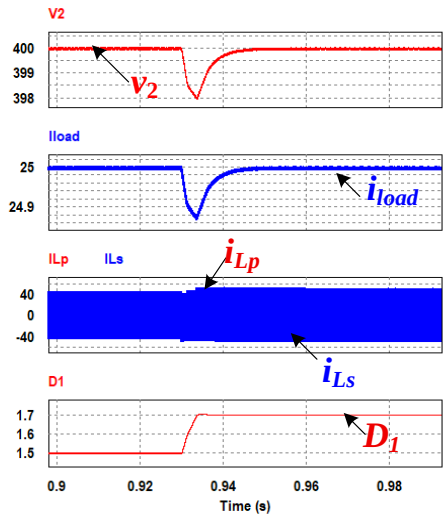

Fig. 10. Simulation results of CC mode when the input source changes from 800 to 700V

Fig. 7 shows the simulation results of CV mode when the load changes 25-50Ω. Fig. 8 presents the simulation results of the CV mode when the input source changes from 800 to 700V. Fig. 9 depicts the simulation results of the CC mode when the load changes 16-14Ω. Fig. 10 shows the simulation results of the CC mode when the input source changes from 800 to 700V

IV. CONCLUSIONS

This paper analyzes the working principle of a DAB converter applied to charging systems, specifically highlighting the soft switching range of switches. A simulation model of the converter was built and operated using PSIM software. The advantage of soft switching capability increases the converter's efficiency, thereby expanding its application range in fields such as energy storage systems, renewable energy systems like solar and wind power, and charging systems for electric vehicles, contributing to the gradual replacement of fossil fuel-powered vehicles with electric vehicles.

REFERENCES

[1] Deshmukh, R.S., Rituraj, G., Bauer, P., and Vahedi, H. "Evaluation and Optimization of Modulation Strategies of a Dual-Active-Bridge Converter for Electrolyzers." *IEEE Open Journal of the Industrial Electronics Society* 7 (2025): 55-71.

[2] Sun, Heyang, et al. "A dynamic response enhanced model predictive control for bidirectional dual active bridge converter." *IEEE Transactions on Industry Applications* (2025).

[3] Sposito, M. and Zurbriggen, I.G. "State-Plane Centric Control of Bidirectional Dual Active Bridge Converters in V2X Applications." *IEEE Transactions on Power Electronics* 40.12 (2025): 18281-18291.

[4] N. M. L. Tan, T. Abe, and H. Akagi, "Design and Performance of a Bidirectional Isolated DC-DC Converter for a Battery Energy Storage System," *IEEE Trans. Power Electron.*, vol. 27, no. 3, pp. 1237–1248, Mar. 2012.

[5] F. Krismer and J. W. Kolar, "Accurate Small-Signal Model for the Digital Control of an Automotive Bidirectional Dual Active Bridge," *IEEE Trans. Power Electron.*, vol. 24, no. 12, pp. 2756–2768, Dec. 2009.

[6] X. She, X. Yu, F. Wang, and A. Q. Huang, "Design and Demonstration of a 3.6-kV-120-V/10-kVA Solid-State Transformer for Smart Grid Application," *IEEE Trans. Power Electron.*, vol. 29, no. 8, pp. 3982–3996, Aug. 2014.

[7] S. Shao *et al.*, "Modeling and Advanced Control of Dual-Active-Bridge DC–DC Converters: A Review," in *IEEE Transactions on Power Electronics*, vol. 37, no. 2, pp. 1524-1547, Feb. 2022, doi: 10.1109/TPEL.2021.3108157.

[8] Anping Tong1,2, Lijun Hang3, Guojie Li1,2, Jingzhou Xu, "Equivalent circuit model of Dual Active Bridge Converter," *IECON 2017 - 43rd Annual Conference of the IEEE Industrial Electronics Society*, December 2017, DOI: 10.1109/IECON.2017.8216806

[9] Yajing Zhang, Hao Ma, Xiuteng Wang, Tiancong Shao, "A power shaping based control strategy for dual active full-bridge converter," *Archives of Electrical Engineering 2024* vol 73 No 2, pp. 543-556, Polish Academy of Sciences, 22.05.2024, DOI: https://doi.org/10.24425/aee.2024.149931

[10] Muhammad Faisal Fiaz, Sandro Calligaro, Mattia Iurich, and Roberto Petrella, "Analytical Modeling and Control of Dual Active Bridge Converter Considering All Phase-Shifts," *Energies 2022*, 15(8), 2720, https://doi.org/10.3390/en15082720, April 2022.

[11] Choi, H.-j.; Lee, W.-b.; Jung, J.-h. Practical Controller Design of Three-Phase Dual Active Bridge Converter for Low Voltage DC Distribution System. *Electronics* **2020**, *9*, 2101. https://doi.org/10.3390/electronics9122101

[12] Sadi, Mohammadhesam Hassani, Zahra Sadeghi, and Jennifer Bauman. "A comprehensive review of universal fast-charging techniques for 400-V and 800-V electric vehicles." *IEEE Access* (2025)